DYNAMIC ANALYSIS OF FUNCTIONALLY GRADED VISCOELASTIC BEAMS ON THE ELASTIC FOUNDATION UNDER MULTIPLE MOVING LOADS

Tran Van Lien[1], **Le Thi Ha**[2,*]
[1]*Hanoi University of Civil Engineering, Hanoi, Vietnam*
[2]*University of Transport and Communications, Hanoi, Vietnam*
*E-mail: lethiha@utc.edu.vn

Abstract. In this paper, the dynamic analysis of the Functionally Graded (FG) simply supported beam resting on the Winkler–Pasternak elastic foundation under multiple moving loads is investigated by using Timoshenko beam theory and the Kelvin–Voigt damping model. The material properties of the FG beam vary continuously in the thickness direction. The Mori–Tanaka homogenization model is used to determine the effective material properties of the FG beam. Equations of motion for the beams are established based on the Finite Element Method (FEM). The effects of different material distributions, velocities of multiple moving loads, distances between loads, and damping on the dynamic responses of the beam are discussed.

Keywords: FGM beam, damping, moving force, Timoshenko beam theory, dynamic behavior.

1. INTRODUCTION

Beams and plates are used in various applications, such as aerospace, marine, automotive, and defense sectors, where continuous elements of these types are required. The necessity for concurrent thermal and mechanical strengths has led to the invention of plate and beam structures with Functionally Graded Material (FGM) properties [1]. The FGM is described by a continuous and smooth variation in both composition profile and material properties along one or more than one direction in order to achieve the desired structural performance [2].

Şimşek [3,4] approximated the displacements using polynomials to evaluate the dynamic response of Functionally Graded (FG) beams subjected to a moving load. Rajabi et al. [5] investigated the influence of a power-law thickness gradation of material properties on the dynamics of an FG Euler–Bernoulli beam excited by a moving oscillator. Using a differential quadrature method, Khalili et al. [6] computed the dynamic response of the FG Euler–Bernoulli beams under a moving load. The material properties of the beams were considered to vary with the beam thickness according to an exponential or a power-law function. Using the Ritz method and Newmark's method, Songsuwan et al. [7] investigated the free and forced vibrations of FG sandwich beams resting on an elastic foundation and under a moving harmonic load. The governing equation of motion for the beam, which includes the effects of shear deformation and rotary inertia based on the Timoshenko beam theory, is derived from Lagrange's equations. By combining the Lagrange method with the Newmark method, Wang and Wu [8] and Wang et al. [9] studied the effects of temperature and porosity on the dynamic behaviors of FG Timoshenko beams and FG sandwich beams under moving loads, respectively. Şimşek and Mohammed [10] investigated the static, free, and forced vibrations of FG sandwich beams under the action of double moving harmonic loads travelling at constant velocities, by using the Timoshenko beam theory.

For the Finite Element Method (FEM), Le et al. [11] studied the vibrations of multi-span FG beams subjected to a moving harmonic load. The material properties of the beam are assumed to vary continuously in the thickness direction by a power-law distribution. The finite element formulation is derived by using the exact solution of the governing differential equations of an FGM Timoshenko beam segment to interpolate the displacements and rotation. The dynamic response of FG beams under a variable velocity moving mass was studied by Esen [12, 13] using first-order shear deformation finite element formulations. By using simple finite element procedures, Esen et al. [14] studied the dynamics of FG Timoshenko beams under a moving mass. The power-law or sigmoid variation was assumed for the beam material properties, and the influence of the foundation support and temperature rise on the dynamics was also considered. Gan et al. [15] derived a two-node Timoshenko beam element for computing the dynamic response of nonuniform axially FG beams. The solution of the equilibrium equations of a beam segment has been employed to interpolate the displacement field, thus improving the efficiency of the element. Nguyen et al. [16] investigated the dynamic behavior of a bidirectional FG sandwich beam under nonuniform motion of a moving load. Based on the first-order shear deformation beam theory, a finite beam element was derived and employed in computing the dynamic response of the beam. Recently, Nguyen et al. [17] has investigated the dynamic analysis of an inclined sandwich beam under a moving mass. A finite element formulation for the inclined beam, in which the stiffness and mass matrices are evaluated explicitly, has been derived by using the transverse shear rotation

as an independent variable. Akbaş et al. [18] analyzed dynamic responses of FG porous thick beams under sin pulse loads by using the Kelvin–Voigt viscoelastic model. Yee et al. [19] studied coupled dynamics of geometrically and material-wise imperfect axially functionally graded graphene nanoplatelets-reinforced viscoelastic shear deformable beams. Cui et al. [20] studied the dynamic response of fractional-order viscoelastic FG beams according to the Kelvin–Voigt fractional derivative model and the quasi-3D beam theory.

In the open literature, the forced vibration of FG viscoelastic beams has not been widely studied. It is observed that most of the dynamic studies of beams are conducted without considering the damping effect. This work addresses forced vibration analysis of a beam by using the Timoshenko beam theory with the Kelvin–Voigt damping model. To solve the dynamic problem, the FEM and Newmark's implicit integration methods are used in the time domain. The effects of material parameters, damping ratios velocies of multiple moving loads, distances between loads, and Winkler–Pasternak elastic foundations on the forced vibration responses of the FG beam are examined and discussed.

2. BASIC RELATIONS

Consider an FGM beam of length L, with a rectangular cross-section $A = b \times h$, resting on a Winkler–Pasternak elastic foundation. The beam is subjected to three loads moving with a constant velocity v from the left end to the right end of the beam (Fig. 1). It is assumed that the three loads are equal and move with the same velocity, and it is always in contact with the beam. Assuming the material volume fraction of the beam varies along the thickness direction as follows

$$V_c(z) = \left(\frac{1}{2} + \frac{z}{h}\right)^n, \quad V_m(z) = 1 - \left(\frac{1}{2} + \frac{z}{h}\right)^n, \quad -\frac{1}{2} \leq \frac{z}{h} \leq \frac{1}{2},$$

where n is the volume fraction index, and z is the coordinates from the mid-plane of the beam; subscripts m and c denote metal and ceramic materials, respectively. Then, the effective bulk modulus K and shear modulus G can be determined from the Mori–Tanaka
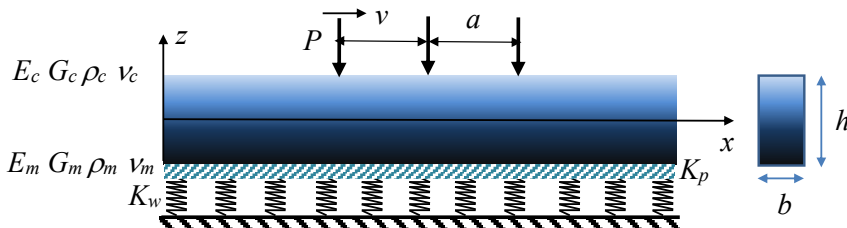

Fig. 1. A FGM beam on a Winkler–Pasternak elastic foundation under multiple moving loads

model as follows

$$K\left(z\right) = K_m + \frac{\left(K_c - K_m\right) V_c(z)}{1 + \left(1 - V_c(z)\right)\left(K_c - K_m\right)/\left(K_m + 4G_m/3\right)},$$

$$G\left(z\right) = G_m + \frac{\left(G_c - G_m\right) V_c(z)}{1 + \dfrac{\left(1 - V_c(z)\right)\left(G_c - G_m\right)}{G_m + G_m\left(9K_m + 8G_m\right)/\left(6K_m + 12G_m\right)}}.$$

The effective material properties of the FGM beam such as Young's modulus E, Poisson's ratio, ν and mass density ρ can be determined as follows

$$E(z) = \frac{9K(z)G(z)}{3K(z) + G(z)}, \quad \nu(z) = \frac{3K(z) - 2G(z)}{2\left[3K(z) + G(z)\right]}, \quad \rho(z) = \rho_c V_c(z) + \rho_m V_m(z).$$

The displacements at a point on the cross-section of the FGM Timoshenko beam can be represented as

$$\begin{aligned}
u(x, z, t) &= u_0(x, t) - (z - h_0)\,\theta(x, t), \\
w(x, z, t) &= w_0(x, t),
\end{aligned} \tag{1}$$

where $u(x, t), w(x, t)$ are the axial displacement, and the deflection of a point on the axis, respectively; θ is the angle of rotation of the cross-section; h is the distance from the neutral axis to the x-axis, h is determined from the condition that the axial force at the cross-section vanishes

$$h_0 = \int_A zE\left(z\right) \mathrm{d}A \bigg/ \int_A E\left(z\right) \mathrm{d}A.$$

The nonzero deformations are obtained as follows

$$\varepsilon_{xx} = \frac{\partial u_0}{\partial x} - (z - h_0)\frac{\partial \theta}{\partial x}, \quad \gamma_{xz} = \frac{\partial w_0}{\partial x} - \theta. \tag{2}$$

Applying the Kelvin–Voigt damping model, the constitutive equations of the FGM beam can be presented as follows [18–20]

$$\begin{aligned}
\sigma_{xx} &= E(z)\varepsilon_{xx} + \varsigma_1 E(z)\dot{\varepsilon}_{xx} = \sigma_{xx(ela)} + \sigma_{xx(vis)}, \\
\sigma_{xz} &= k_s G(z)\gamma_{xz} + k_s \varsigma_2 G(z)\dot{\gamma}_{xz} = \sigma_{xy(ela)} + \sigma_{xy(vis)},
\end{aligned} \tag{3}$$

where k_s is the shear correction coefficient, $k_s = 5/6$ for a rectangular cross-section; ς_1, ς_2 are the damping ratios in bending and shearing, respectively; the "*elas*" and "*vis*" subscripts denote the elastic and viscoelastic stress parts, respectively.

Using expressions (1), (2) and (3), the strain energy U the kinetic energy T and the dissipation function R of the FG beam can be obtained as follows [18–20]

$$
\begin{aligned}
U &= \int_0^L \int_A \left(\sigma_{xx(ela)} \varepsilon_{xx} + \sigma_{xz(ela)} \gamma_{xz} \right) \mathrm{d}A \mathrm{d}x \\
&= \frac{1}{2} \int_0^L \left[A_{11} \left(\frac{\partial u_0}{\partial x} \right)^2 - 2 A_{12} \frac{\partial u_0}{\partial x} \frac{\partial \theta}{\partial x} + A_{22} \left(\frac{\partial \theta}{\partial x} \right)^2 + k_s A_{33} \left(\frac{\partial w_0}{\partial x} - \theta \right)^2 \right] \mathrm{d}x,
\end{aligned}
\tag{4}
$$

$$
\begin{aligned}
T &= \frac{1}{2} \int_0^L \int_A \rho(z) \left[\left(\frac{\partial u}{\partial t} \right)^2 + \left(\frac{\partial w}{\partial t} \right)^2 \right] \mathrm{d}A \mathrm{d}x \\
&= \frac{1}{2} \int_0^L \left\{ I_{11} \left[\left(\frac{\partial u_0}{\partial t} \right)^2 + \left(\frac{\partial w_0}{\partial t} \right)^2 \right] - 2 I_{12} \frac{\partial u_0}{\partial t} \frac{\partial \theta}{\partial t} + I_{22} \left(\frac{\partial \theta}{\partial t} \right)^2 \right\} \mathrm{d}x,
\end{aligned}
\tag{5}
$$

where A_{11}, A_{12}, A_{22} A_{33} are the rigidities and I_{11}, I_{12}, I_{22} are the mass moments, respectively

$$
(A_{11}, A_{12}, A_{22}) = \int_A E(z) \left[1, z - h_0, (z - h_0)^2 \right] \mathrm{d}A, \quad A_{33} = \int_A G(z) \mathrm{d}A,
$$

$$
(I_{11}, I_{12}, I_{22}) = \int_A \rho(z) \left[1, z - h_0, (z - h_0)^2 \right] \mathrm{d}A,
$$

and

$$
\begin{aligned}
R &= \int_0^L \int_A \left(\sigma_{xx(vis)} \dot{\varepsilon}_{xx} + \sigma_{xz(vis)} \dot{\gamma}_{xz} \right) \mathrm{d}A \mathrm{d}x \\
&= \frac{1}{2} \int_0^L \left[C_{11} \left(\frac{\partial \dot{u}_0}{\partial x} \right)^2 - 2 C_{12} \frac{\partial \dot{u}_0}{\partial x} \frac{\partial \dot{\theta}}{\partial x} + C_{22} \left(\frac{\partial \dot{\theta}}{\partial x} \right)^2 + k_s C_{33} \left(\frac{\partial \dot{w}_0}{\partial x} - \dot{\theta} \right)^2 \right] \mathrm{d}x,
\end{aligned}
\tag{6}
$$

where C_{11}, C_{12}, C_{22} and C_{33} are the damping coefficients, respectively

$$
(C_{11}, C_{12}, C_{22}) = \int_A E(z) \varsigma_1(z) \left[1, z - h_0, (z - h_0)^2 \right] \mathrm{d}A,
$$

$$
C_{33} = \int_A G(z) \varsigma_2(z) \, \mathrm{d}A.
$$

The strain energy of the Winkler–Pasternak foundation

$$
U_F = \frac{1}{2} \int_0^L \left[K_w w^2 + K_p \left(\frac{\partial w}{\partial x} \right)^2 \right] \mathrm{d}x,
\tag{7}
$$

where K_w, K_p are the Winkler–Pasternak elastic foundation coefficients.

The potential energy of the external load P is given as follows

$$V = - \sum_{i=1}^{nload} \int_0^L P w_p \left(x_p \right) \delta \left(x_p - v t_i \right) dx, \tag{8}$$

where $\delta(.)$ is the Dirac delta function, x_p is the current abscissa of the load P with respect to the left end of the beam, w_p is the deflection at the position of force P, t denotes the time variable

3. FINITE ELEMENT FORMULATION

By using the FEM, the beam is assumed to be divided into numbers of two-node beam elements of length L. The vector of nodal displacements $\mathbf{d}$ for the element, considering the transverse shear rotation θ as an independent variable, contains six components as follows

$$\mathbf{d} = \left\{ u_i, w_i, \theta_i, u_j, w_j, \theta_j \right\}^T, \tag{9}$$

where i and j denote the left and right nodes, respectively. In Eq. (9) and hereafter, a superscript 'T' is used to denote the transpose of a vector or a matrix. The displacement and rotation angles of the FGM Timoshenko beam element can be interpolated as follows

$$\left\{ \begin{matrix} u_0 \\ w_0 \\ \theta \end{matrix} \right\} = \begin{bmatrix} N_u^1 & 0 & 0 & N_u^2 & 0 & 0 \\ 0 & N_w^1 & N_w^2 & 0 & N_w^3 & N_w^4 \\ 0 & N_\theta^1 & N_\theta^2 & 0 & N_\theta^3 & N_\theta^4 \end{bmatrix} \left\{ u_i \ \ w_i \ \ \theta_i \ \ u_j \ \ w_j \ \ \theta_j \right\}^T = \begin{bmatrix} \mathbf{N}_u \\ \mathbf{N}_w \\ \mathbf{N}_\theta \end{bmatrix} \mathbf{d},$$

where N_u^1, N_u^2 are Lagrange's shape functions of the axial displacement

$$N_u^1 = 1 - \frac{x}{L}, \quad N_u^2 = \frac{x}{L},$$

$N_w^1, N_w^2, N_w^3, N_w^4$ and $N_\theta^1, N_\theta^2, N_\theta^3, N_\theta^4$ are Kosmatka's shape functions [21].

Using the above interpolations, the strain energy of the beam in Eq. (4) can be written as

$$U = \frac{1}{2} \sum^{n_e} \mathbf{d}^T \mathbf{k}_b^e \mathbf{d},$$

where n_e is the total number of elements used to discretize the beam; and $\mathbf{k}_b^e$ is the beam element stiffness matrix,

$$\mathbf{k}_b^e = \mathbf{k}_{11} + \mathbf{k}_{12} + \mathbf{k}_{22} + \mathbf{k}_{33},$$

$$\mathbf{k}_{11} = \int_0^L \left(\frac{\partial \mathbf{N}_u}{\partial x} \right)^T A_{11} \frac{\partial \mathbf{N}_u}{\partial x} dx, \quad \mathbf{k}_{12} = -2 \int_0^L \left(\frac{\partial \mathbf{N}_u}{\partial x} \right)^T A_{12} \frac{\partial \mathbf{N}_\theta}{\partial x} dx,$$

$$\mathbf{k}_{22} = \int_0^L \left(\frac{\partial \mathbf{N}_\theta}{\partial x}\right)^T A_{22} \frac{\partial \mathbf{N}_\theta}{\partial x} dx, \quad \mathbf{k}_{33} = k_s \int_0^L \left(\frac{\partial \mathbf{N}_w}{\partial x} - \mathbf{N}_\theta\right)^T A_{33} \left(\frac{\partial \mathbf{N}_w}{\partial x} - \mathbf{N}_\theta\right) dx.$$

The kinetic energy of the beam in Eq. (5) can be written in the following form

$$T = \frac{1}{2} \sum_{}^{n_e} \dot{\mathbf{d}}^T \mathbf{m}^e \dot{\mathbf{d}},$$

where the element mass matrix of the beam $\mathbf{m}^e$

$$\mathbf{m}^e = \mathbf{m}_{11} + \mathbf{m}_{12} + \mathbf{m}_{22} + \mathbf{m}_{33},$$

$$\mathbf{m}_{11} = \int_0^L \left(\frac{\partial \mathbf{N}_u}{\partial x}\right)^T A_{11} \frac{\partial \mathbf{N}_u}{\partial x} dx, \quad \mathbf{m}_{12} = \int_0^L \left(\frac{\partial \mathbf{N}_u}{\partial x}\right)^T A_{12} \frac{\partial \mathbf{N}_\theta}{\partial x} dx,$$

$$\mathbf{m}_{22} = \int_0^L \left(\frac{\partial \mathbf{N}_w}{\partial x}\right)^T A_{11} \frac{\partial \mathbf{N}_w}{\partial x} dx, \quad \mathbf{m}_{33} = \int_0^L \left(\frac{\partial \mathbf{N}_\theta}{\partial x}\right)^T A_{22} \frac{\partial \mathbf{N}_\theta}{\partial x} dx.$$

Similarly, the dissipation function of the beam in Eq. (6) can be written as

$$R = \frac{1}{2} \sum_{}^{ne} \dot{\mathbf{d}}^T \mathbf{c}^e \dot{\mathbf{d}},$$

where $\mathbf{c}^e$ is the damping matrix of the Timoshenko beam element

$$\mathbf{c}^e = \mathbf{c}_{11} + \mathbf{c}_{12} + \mathbf{c}_{22} + \mathbf{c}_{33},$$

$$\mathbf{c}_{11} = \int_0^L \left(\frac{\partial \mathbf{N}_u}{\partial x}\right)^T C_{11} \frac{\partial \mathbf{N}_u}{\partial x} dx, \quad \mathbf{c}_{12} = -2 \int_0^L \left(\frac{\partial \mathbf{N}_u}{\partial x}\right)^T C_{12} \frac{\partial \mathbf{N}_\theta}{\partial x} dx,$$

$$\mathbf{c}_{22} = \int_0^L \left(\frac{\partial \mathbf{N}_\theta}{\partial x}\right)^T C_{22} \frac{\partial \mathbf{N}_\theta}{\partial x} dx, \quad \mathbf{c}_{33} = k_s \int_0^L \left(\frac{\partial \mathbf{N}_w}{\partial x} - \mathbf{N}_\theta\right)^T C_{33} \left(\frac{\partial \mathbf{N}_w}{\partial x} - \mathbf{N}_\theta\right) dx.$$

The strain energy of the Winkler–Pasternak elastic foundation in Eq. (7) can be written in a matrix form as

$$U_F = \frac{1}{2} \sum_{}^{n_e} \mathbf{d}^T \mathbf{k}_F^e \mathbf{d},$$

$\mathbf{k}_F^e$ is the element foundation stiffness matrix with the following form

$$\mathbf{k}_F^e = k_{e,w} + k_{e,p}, \quad k_{e,w} = \frac{1}{2} \int_0^L \mathbf{N}_w^T K_w \mathbf{N}_w dx, \quad k_{e,p} = \frac{1}{2} \int_0^L \left(\frac{\partial \mathbf{N}_w}{\partial x}\right)^T K_p \frac{\partial \mathbf{N}_w}{\partial x} dx.$$

The total stiffness matrix $(\mathbf{k})$ for the element with the foundation support is as follows

$$\mathbf{k}^e = \mathbf{k}_b^e + \mathbf{k}_F^e.$$

For the element without the foundation support, the matrix $\mathbf{k}$ is simply given by $\mathbf{k}^e = \mathbf{k}_b^e$.

The matrix form for the potential energy in Eq. (8) is as follows

$$V = -\sum_{}^{ne} \mathbf{d}^T \mathbf{f}^e,$$

where $\mathbf{f}^e$ is the element time-dependent nodal load vector. $\mathbf{f}^e$ has zero coefficients, except for the element

$$\mathbf{f}^e = \sum_{i=1}^{nload} P_i \left(\mathbf{N}_w\right)^T \bigg|_{x_P},$$

x_p is the current abscissa of the moving load P_i with respect to the left end of the beam.

The discretized equations of motion for vibration analysis of the beam can be written in the following form [22]

$$-\frac{\mathrm{d}}{\mathrm{d}t}\left(\frac{\partial T}{\partial \dot{d}_j}\right) + \frac{\partial\left(T - U - U_F - V\right)}{\partial d_j} - \frac{\partial R}{\partial \dot{d}_j} = 0.$$

They can be put in the matrix form as follows

$$\mathbf{M\ddot{D}} + \mathbf{C\dot{D}} + \mathbf{KD} = \mathbf{F}, \tag{10}$$

in which $\mathbf{\ddot{D}}, \mathbf{\dot{D}}, \mathbf{D}$ are the global vectors of nodal displacements, velocity, and accelerations, respectively; $\mathbf{K}, \mathbf{C}, \mathbf{M}$, and $\mathbf{F}$ are the global stiffness, damping mass matrices, and the moving load vector, respectively. These matrices are obtained by assembling the matrices $\mathbf{k}^e, \mathbf{c}^e, \mathbf{m}^e$, and vector $\mathbf{f}^e$ over the elements

$$\mathbf{M} = \sum_{n_e} \mathbf{m}^e, \quad \mathbf{C} = \sum_{n_e} \mathbf{c}^e, \quad \mathbf{K} = \sum_{n_e} \mathbf{k}^e, \quad \mathbf{F} = \sum_{n_e} \mathbf{f}^e.$$

Eq. (10) can be solved by Newmark's implicit integration method. The average acceleration method, which ensures the unconditional convergence of the numerical solution is adopted herein.

4. NUMERICAL RESULTS AND DISCUSSION

For convenience, the maximum normalized dynamic deflection at the mid-span of the simply supported beam $w(L/2, t)/w_0$, the dynamic magnification factor f_D and the nondimensional Winkler–Pasternak elastic foundation coefficients k_w, k_p are introduced as follows

$$f_D = \max\left[\frac{w(L/2, t)}{w_0}\right], \quad w_0 = \frac{PL^3}{48E_m I}, \quad k_w = \frac{K_w L^4}{E_m I}, \quad k_p = \frac{K_p L^2}{E_m I}, \quad I = \frac{bh^3}{12},$$

where w_0 is the static midspan deflection when the load P is at the midspan of the beam.

4.1. Validations

The accuracy of the proposed FEM solution is validated through comparison studies. Firstly, the dynamic deflection at the mid-span of the simply supported beam without damping, subjected to three moving loads is compared with the result of Henchi [23] in Fig. 2, for the cases where the distance between the loads $a = L/8$ m (Fig. 2(a)), $v = 22.5$ m/s and $a = L/4$ m (Fig. 2(b)). The good agreement between the present results with those of the cited reference is shown in the figure.
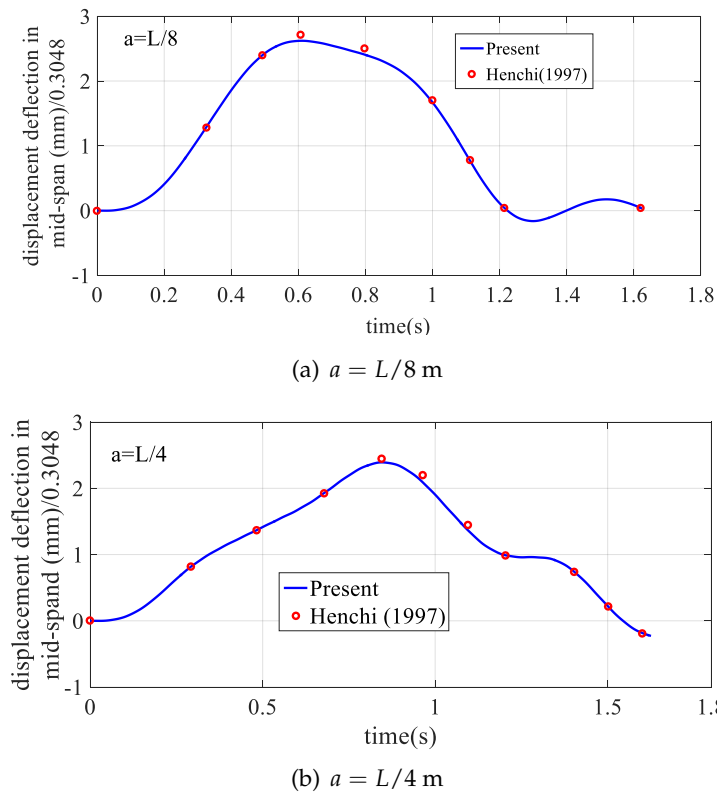

(a) $a = L/8$ m

(b) $a = L/4$ m

Fig. 2. Comparison of the dynamic deflection at the mid-span of the beam, for different values of the distance a between the three moving loads at $v = 22.5$ m/s

The second comparison of the dynamic magnification factor f_D of the FGM beams and the corresponding critical moving load velocities, for the different volume fraction indexes n with those of Şimşek and Kocatürk [4], is presented in Table 1. The excellent agreement between the present and published solutions is shown. These above comparisons validate that the proposed FEM solutions are both acceptable and reliable.

Table 1. Comparison of the dynamic magnification factor f_D of FGM beams, and the corresponding critical moving load velocities with the different volume fraction indexes n

n	f_D Present	Critical velocity Present (m/s)	f_D Şimşek [4]	Critical velocity Şimşek [4] (m/s)
0.2	1.0647	221	1.0647	220
0.5	1.1815	196	1.1816	194
1.0	1.2828	177	1.2828	175
2.0	1.3648	163	1.3648	161

4.2. Parametric study

The influence of damping on dynamic responses of a simply supported FG beam under multiple moving loads is numerically studied in this section. The FGM beam consists of steel and Alumina (Al_2O_3) with material properties [4] E_m = 210 GPa, ρ_m = 7800 kg/m^3 for steel; E_c = 390 GPa, ρ_c = 3960 kg/m^3 for Alumina (Al_2O_3), is considered. The geometrical parameters of the beam are as follows [4]: the height $h = 0.9$ m, the width $b = 0.4$ m and various values of the aspect ratio L/h. Moreover, since studies on viscoelastic beams are rare to choose the damping ratio, so in this study the damping ratios ς_1, ς_2, and ς_3 are assumed to have the same value ($\varsigma_1 = \varsigma_2 = \varsigma_3 = \varsigma$), within the interval from 0 to 10^{-1}.

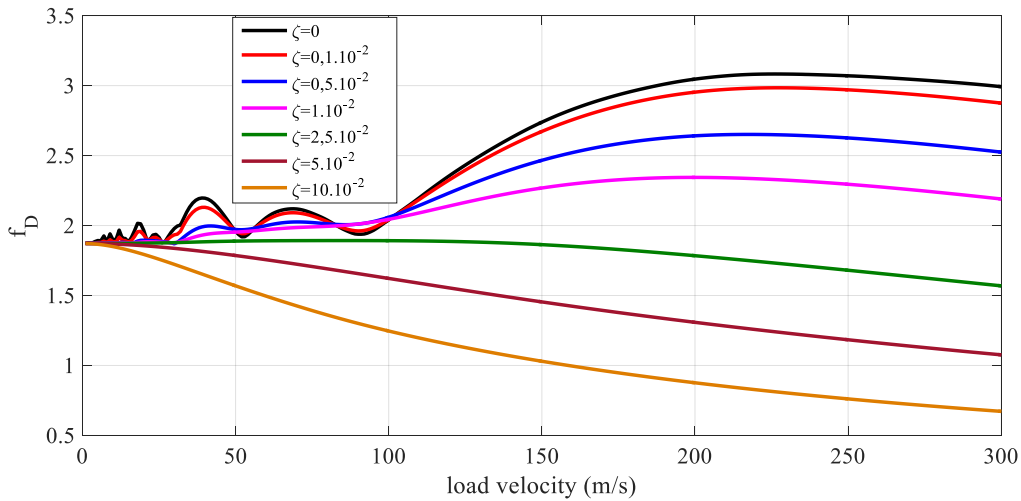*Fig. 3.* The dynamic magnification factor of the FG beam, subjected to three loads where $n = 2, L/h = 20, k_w = 0, k_p = 0$, and $a = L/4$ with different damping ratios

Fig. 3 illustrates the influence of the damping ratio on the dynamic magnification factor at the mid-span of the FG beam, without the elastic foundation subjected to a moving convoy of three moving loads with the volume fraction index $n = 2$, the ratio of the

length to the height $L/h = 20$, and the distance between the loads $a = L/4$. The result shows that an increase in the damping ratio decreases the dynamic magnification factor values and the number of associated oscillations of the dynamic magnification factor for all values of the moving load velocity. When the damping ratio is less than or equal to 1×10^{-2} ($\varsigma \leq 1 \times 10^{-2}$), a critical moving load velocity causes the dynamic magnification factor to reach the maximum. Moreover, the maximum dynamic magnification factor and the moving load velocity, which are required to reach the maximum value, are decreased while the damping ratios increase. When the damping ratio is greater than 5×10^{-2} ($\varsigma > 5 \times 10^{-2}$), the dynamic magnification factor decreases monotonously at all moving load velocity values.

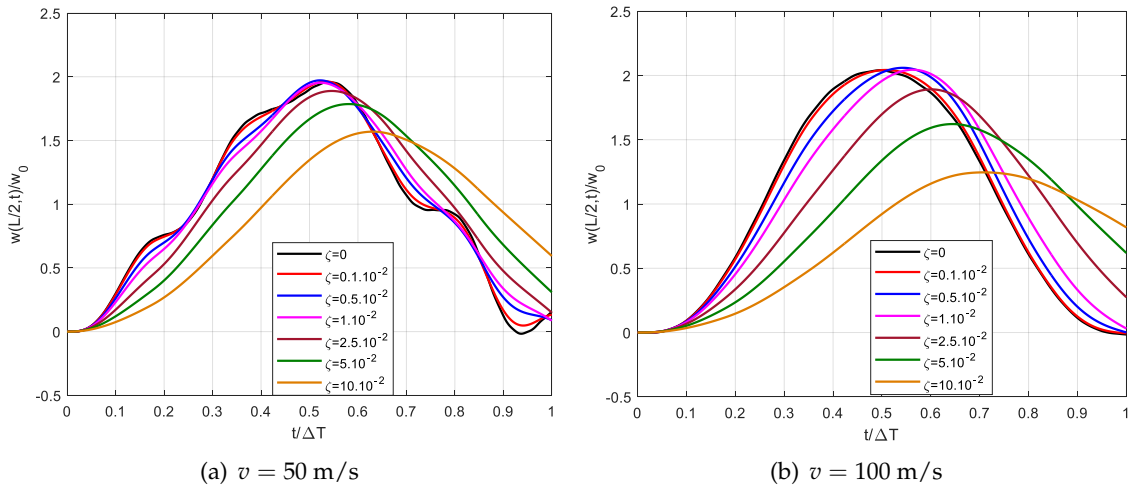(a) $v = 50$ m/s   (b) $v = 100$ m/s

Fig. 4. The normalized dynamic deflection at the midspan of the FG beam
in case of $n = 2, L/h = 20, k_w = 0, k_p = 0, a = L/4$

Fig. 4 depicts the influence of damping ratios on the normalized dynamic deflection at the mid-span of the FG beam, subjected to a moving convoy of three loads with $n = 2, L/h = 20, k_w = 0, k_p = 0$, the distance between the loads $a = L/4$ where the velocity loads a) $v = 50$ m/s (Fig. 4(a)), $v = 100$ m/s (Fig. 4(b)), in which ΔT is the total time necessary for the moving loads to cross the beam. Fig. 5 shows the influence of damping ratios on the normalized dynamic defection at the midspan of the FG beam under one moving load (Fig. 5(a)), and three moving loads (Fig. 5(b)), and the velocity loads $v = 25$ (m/s), $n = 2, L/h = 20, k_w = 0, k_p = 0$, the distance between the loads $a = L/4$. By observing the graphs presented in Figs. 4–5, it allows one to make the following remarks:
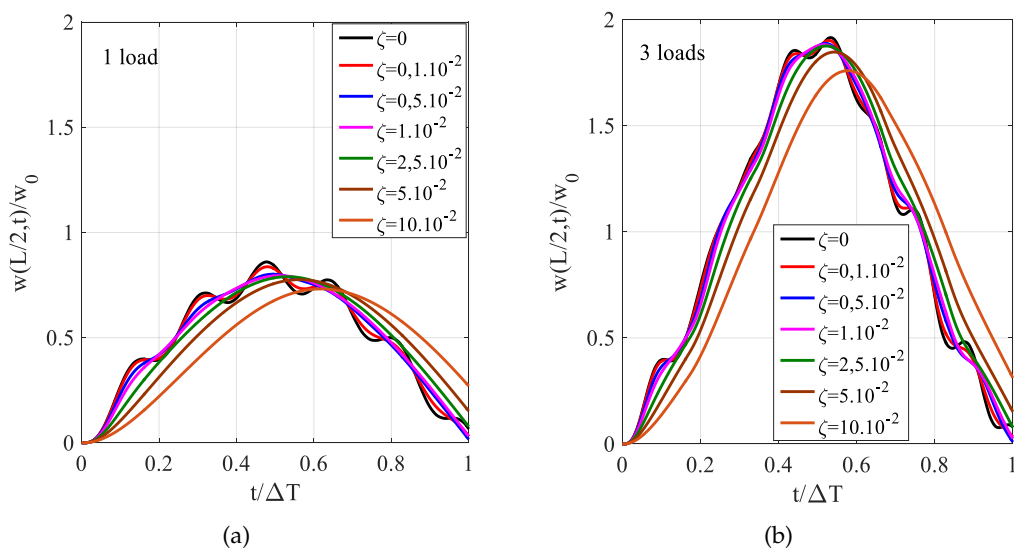
Fig. 5. The normalized dynamic defection at the midspan of the FG beam, subjected to
(a) 1 load, (b) 3 loads with $v = 25$ (m/s), $a = L/4, n = 2, L/h = 20, k_w = 0, k_p = 0$

- Increasing the damping ratio decreases the maximum value of the normalized dynamic deflection at the mid-span of the simply supported beam.

- The beam exhibits the associated oscillations with higher frequencies when the damping ratios are less than 1×10^{-2}. Lower moving load velocity and the damping ratios result in higher frequency oscillations.

- Increasing the number of moving loads increases the maximum value of the normalized dynamic deflection at the mid-span of the simply supported beam. However, higher numbers of moving loads result in the lower amplitudes of associated oscillations.

Fig. 6 shows the influence of the moving load velocity on the normalized dynamic deflection at the midspan of the FG beam, subjected to a moving convoy of three loads with two damping ratios, $\varsigma = 0$ (Fig. 6(a)) and $\varsigma = 0.5 \times 10^{-2}$ (Fig. 6(b)) and $n = 2, L/h = 20, k_w = 0, k_p = 0$, the distance between the loads $a = L/4$. Increasing the moving load velocity or decreasing the damping ratio increases the maximum values of the dynamic deflection at the midspan. However, the increase of the damping ratio reduces the associated oscillations of the dynamic deflection at the midspan while the time required to reach the maximum value of these oscillations are increased.

The dynamic deflection at the midspan of the beam, subjected to a moving convoy of three loads for various values of the distance *a* between the loads, is presented in Fig. 7 with $n = 2, L/h = 20$, the moving load velocity $v = 25$ m/s, and damping ratios: $\varsigma = 0$

(a) $\varsigma = 0$ (b) $\varsigma = 0.5 \times 10^{-2}$
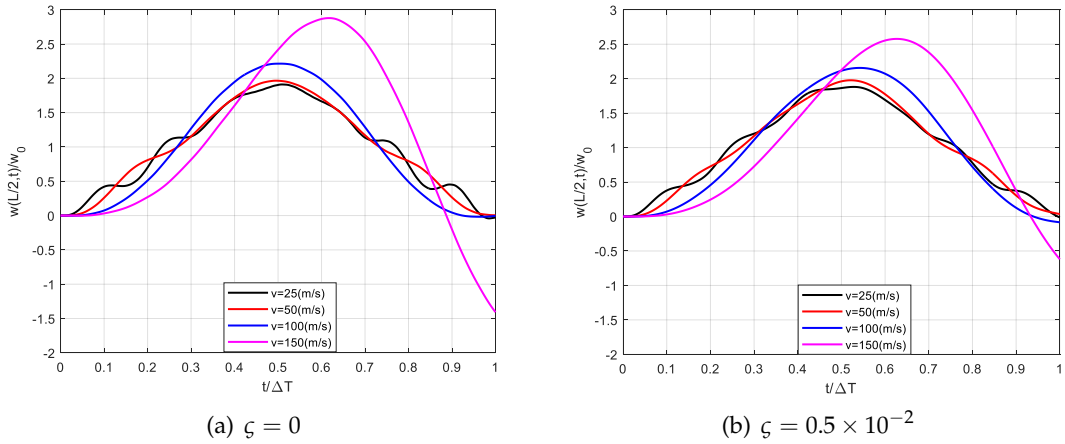
Fig. 6. The normalized dynamic deflection at the midspan of the FG beam is subjected to 3 loads in case of $n = 2, L/h = 20, k_w = 0, k_p = 0, a = L/4$ with damping ratios
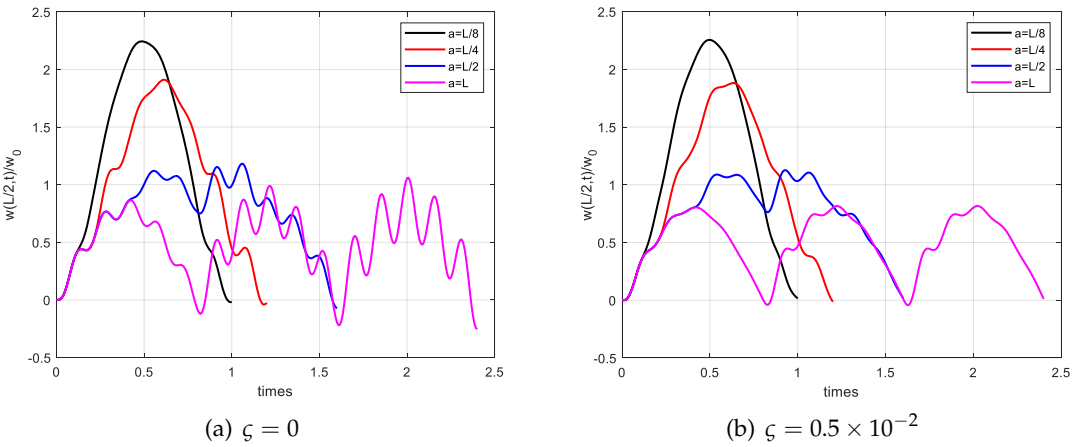

(a) $\varsigma = 0$ (b) $\varsigma = 0.5 \times 10^{-2}$

Fig. 7. The dynamic deflection at the midspan of the beam for values of a between the three moving loads at $n = 2, L/h = 20, k_w = 0, k_p = 0, v = 25$ m/s with damping ratios

(Fig. 7(a)) and $\varsigma = 0.5 \times 10^{-2}$ (Fig. 7(b)). Increasing the distance *a* between the loads and the damping ratio decreases the maximum value and the number of associated oscillations of the normalized dynamic deflection at the midspan. Furthermore, the period of the major oscillations depends on the distance between the loads.

Fig. 8 illustrates the influence of the number of moving loads on the normalized dynamic deflection at the midspan of the FG beam with two damping ratios: $\varsigma = 0$ (Fig. 8(a)) and $\varsigma = 0.5 \times 10^{-2}$ (Fig. 8(b)) and $n = 2, L/h = 20, k_w = 0, k_p = 0$, and the distance between the loads $a = L/4$. Increasing the number of moving loads on the

beam increases the maximum values in the dynamic deflection at the midspan of the beam but these values do not increase uniformly with the number of loads. For example, the maximum value in the dynamic deflection has values of 0.867, 1.512, 1.911, and 2.084 corresponding to the number of loads of 1, 2, 3, and 4 when the damping ratio is equal to 0. Moreover, increasing the number of moving loads on the beam or the damping ratio decreases the number of the associated oscillations of the dynamic deflection at the midspan of the beam. The period of major oscillations increases when the number of moving loads increases.
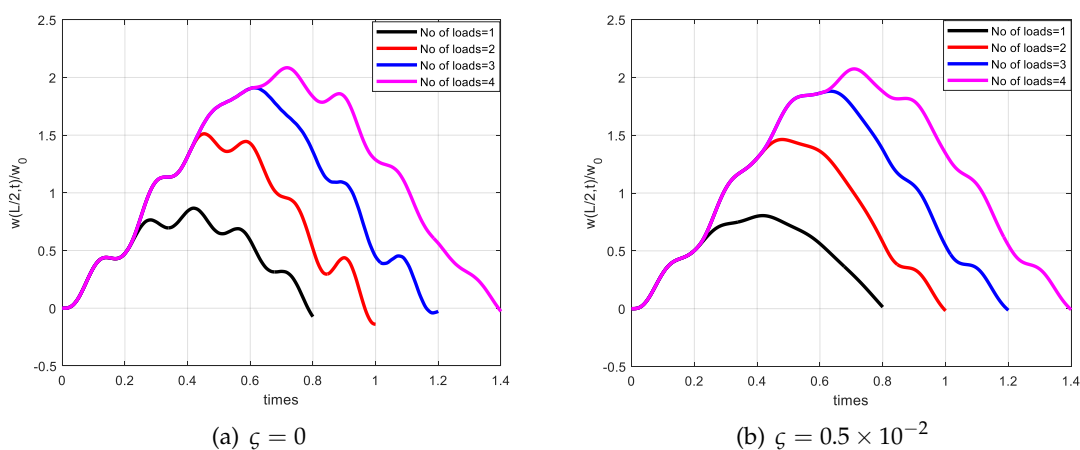

(a) $\varsigma = 0$ (b) $\varsigma = 0.5 \times 10^{-2}$

Fig. 8. The dynamic deflection at the midspan of the beam for values of number of moving loads at $n = 2, L/h = 20, k_w = 0, k_p = 0, a = L/4, v = 25$ m/s with damping ratios

Fig. 9 shows the influence of the volume fraction index n on the dynamic magnification factor f_D of the FG beam subjected to three loads with the damping ratio: $\varsigma = 0$ (Fig. 9(a)), $\varsigma = 0.5 \times 10^{-2}$ (Fig. 9(b)) and $L/h = 20, k_w = 0, k_p = 0, a = L/4$. When the velocity increases from 0 to 100 (m/s), the amplitude of normalized dynamic deflection at the midspan of the FG beam varies continuously, especially when the damping ratio is small. It is shown that the dynamic magnification factor of the FG beam increases remarkably when the damping ratios decrease or the n increases.

Fig. 10 depicts the influence of Winkler elastic foundation coefficients k_w on the dynamic magnification factor of the FG beam subjected to three loads with the Pasternak coefficient $k_p = 0$ at the damping ratio $\varsigma = 0$ (Fig. 10(a)) and $\varsigma = 0.5 \times 10^{-2}$ (Fig. 10(b)), and $L/h = 20, k_p = 0$, and the distance between the loads $a = L/4$. It is shown that the dynamic magnification factor of the FG beam decreases when the Winkler elastic foundation coefficients and the damping ratios increase. When the velocity increases from 0 to 100 (m/s), the dynamic magnification factor of the FG beam varies continuously in case the damping ratio is equal to 0.
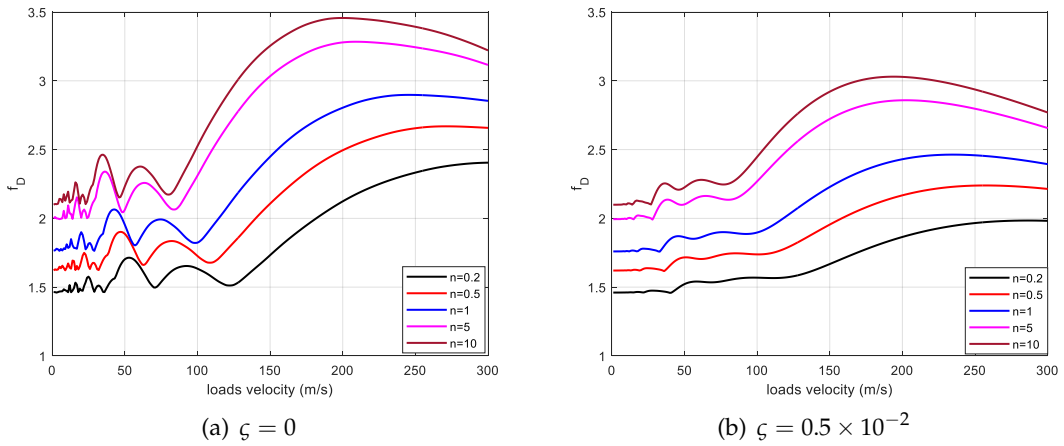
(a) $\varsigma = 0$ (b) $\varsigma = 0.5 \times 10^{-2}$

Fig. 9. The dynamic magnification factor of the FG beam subjected to three loads,
in case of $L/h = 20, k_w = 0, k_p = 0, a = L/4$ with damping ratios

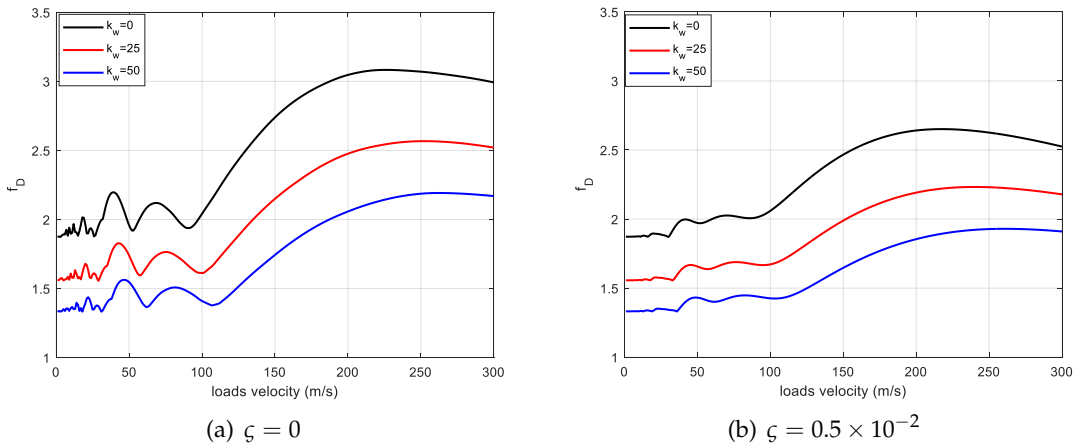(a) $\varsigma = 0$ (b) $\varsigma = 0.5 \times 10^{-2}$

Fig. 10. The dynamic magnification factor of the FG beam subjected to three loads,
where $L/h = 20, k_p = 0, a = L/4$ with damping ratios

Fig. 11 illustrates the influence of Pasternak elastic foundation coefficients k_p on the dynamic magnification factor of the FG beam with the Winkler coefficient $k_w = 0$ at the damping ratio $\varsigma = 0$ (Fig. 11(a)) and $\varsigma = 0.5 \times 10^{-2}$ (Fig. 10(b)), $L/h = 20$, and the distance between the loads $a = L/4$. It is noted that the dynamic magnification factor of the FG beam decreases when the Pasternak elastic foundation coefficients and the damping ratios increase. Furthermore, the dynamic magnification factor of the FG beam varies continuously when the velocity increases from 0 to 100 (m/s) and the damping ratio is equal to 0.
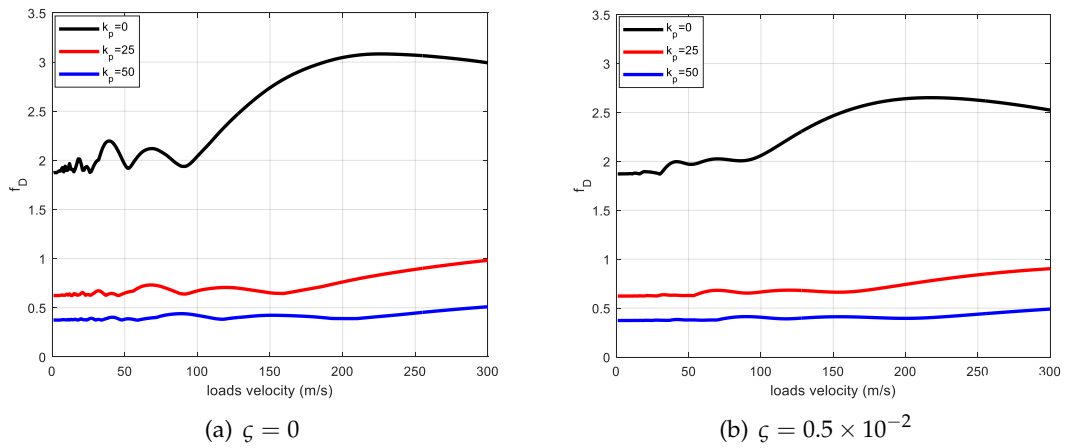
(a) $\varsigma = 0$ (b) $\varsigma = 0.5 \times 10^{-2}$

Fig. 11. The dynamic magnification factor of the FG beam subjected to three loads, where $L/h = 20, k_w = 0, a = L/4$ with damping ratios

(a) $\varsigma = 0$ (b) $\varsigma = 0.5 \times 10^{-2}$
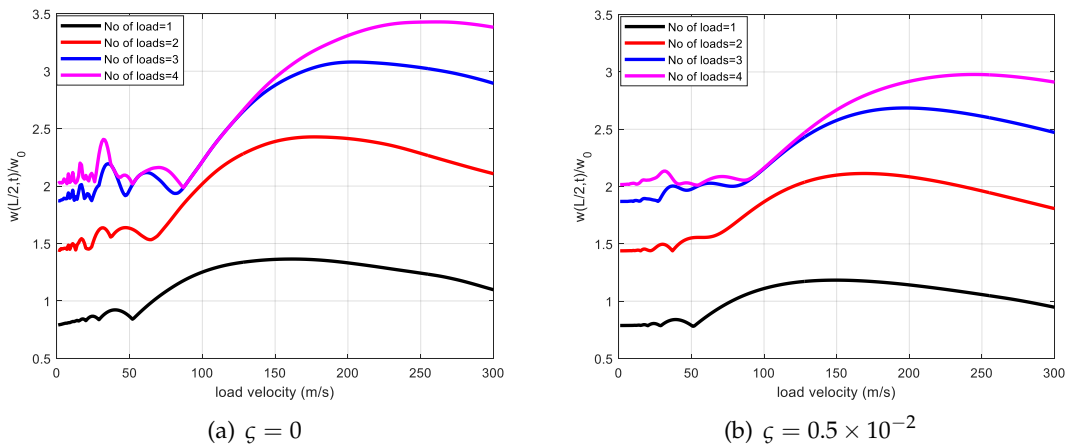
Fig. 12. The dynamic magnification factor of the FG beam, where $L/h = 20$, $k_w = 0, k_p = 0, a = L/4$ with damping ratios

Fig. 12 shows the influence of the number of moving loads on the dynamic magnification factor at the midspan of the FG beam with two damping ratios, $\varsigma = 0$ (Fig. 12(a)) and $\varsigma = 0.5 \times 10^{-2}$ (Fig. 12(b)) and $n = 2, L/h = 20, k_w = 0, k_p = 0$, and the distance between the loads $a = L/4$. The dynamic magnification factor increases when the number of moving loads on the beam increases but the value of the dynamic magnification factor does not increase uniformly with the number of loads. Moreover, the dynamic magnification factor of the FG beam varies continuously when the velocity increases from 0 to 100 (m/s) and the damping ratio is equal to 0.

5. CONCLUSIONS

In this study, the dynamic analysis of the FG viscoelastic beam resting on the Winkler–Pasternak elastic foundation under multiple moving loads has been presented. The finite element method and the Newmark implicit integration methods are used in the time domain. The influences of the geometry, damping, the distance between the loads, velocity parameters, and material parameters on forced vibration responses of the functionally graded beams are investigated. The results obtained in this study are well agreed with those published in earlier references. The most important points from this work can be summarized as follows:

- The damping parameter, the distance between loads, the number of moving loads, and the velocity parameter play key roles in the vibration characteristics of the beam

- Increasing the damping ratio reduces both the dynamic magnification factor values and the number of associated oscillations of the dynamic magnification factor for all values of the moving load velocity, although the moving load velocity is a significant factor to the dynamic response of FG the beam.

- When the damping ratio is less than 1×10^{-2}, a critical velocity exists to make the dynamic magnification factor reach its maximum. The maximum dynamic magnification factor and the moving load velocity required to reach the maximum value are decreased while the damping ratios increase. The dynamic magnification factor of the FG beam varies continuously when the velocity is from 0 to 100 (m/s) and the damping ratio is equal to 0.

- Increasing the distance a between the loads decreases the maximum value and the number of associated oscillations of the normalized dynamic deflection at the midspan of the beam.

- Increasing the number of moving loads increases the maximum values in the dynamic deflection at the midspan of the beam but the dynamic magnification factor does not increase uniformly with the number of loads. Furthermore, the period of major oscillations increases when the number of moving loads increases.

- The effect of the velocity of the moving load can be effectively reduced when the Winkler–Pasternak elastic foundation coefficients increase.

Numerical results show that the above-mentioned effects play an important role in the dynamic deflections of the beam.

DECLARATION OF COMPETING INTEREST

The authors declare that they have no known competing financial interests or personal relationships that could have appeared to influence the work reported in this paper.

ACKNOWLEDGMENT

REFERENCES

[1] M. H. Ghayesh. Resonant dynamics of axially functionally graded imperfect tapered Timoshenko beams. *Journal of Vibration and Control*, **25**, (2018), pp. 336–350. https://doi.org/10.1177/1077546318777591.

[2] S. Zhao, Z. Yang, S. Kitipornchai, and J. Yang. Dynamic instability of functionally graded porous arches reinforced by graphene platelets. *Thin-Walled Structures*, **147**, (2020). https://doi.org/10.1016/j.tws.2019.106491.

[3] M. Şimşek. Vibration analysis of a functionally graded beam under a moving mass by using different beam theories. *Composite Structures*, **92**, (2010), pp. 904–917. https://doi.org/10.1016/j.compstruct.2009.09.030.

[4] M. Şimşek and T. Kocatürk. Free and forced vibration of a functionally graded beam subjected to a concentrated moving harmonic load. *Composite Structures*, **90**, (4), (2009), pp. 465–473. https://doi.org/10.1016/j.compstruct.2009.04.024.

[5] K. Rajabi, M. H. Kargarnovin, and M. Gharini. Dynamic analysis of a functionally graded simply supported Euler–Bernoulli beam subjected to a moving oscillator. *Acta Mechanica*, **224**, (2013), pp. 425–446. https://doi.org/10.1007/s00707-012-0769-y.

[6] S. M. R. Khalili, A. A. Jafari, and S. A. Eftekhari. A mixed Ritz-DQ method for forced vibration of functionally graded beams carrying moving loads. *Composite Structures*, **92**, (2010), pp. 2497–2511. https://doi.org/10.1016/j.compstruct.2010.02.012.

[7] W. Songsuwan, M. Pimsarn, and N. Wattanasakulpong. Dynamic responses of functionally graded sandwich beams resting on elastic foundation under harmonic moving loads. *International Journal of Structural Stability and Dynamics*, **18**, (2018). https://doi.org/10.1142/s0219455418501122.

[8] Y. Wang and D. Wu. Thermal effect on the dynamic response of axially functionally graded beam subjected to a moving harmonic load. *Acta Astronautica*, **127**, (2016), pp. 171–181. https://doi.org/10.1016/j.actaastro.2016.05.030.

[9] Y. Wang, A. Zhou, T. Fu, and W. Zhang. Transient response of a sandwich beam with functionally graded porous core traversed by a non-uniformly distributed moving mass. *International Journal of Mechanics and Materials in Design*, **16**, (2020), pp. 519–540. https://doi.org/10.1007/s10999-019-09483-9.

[10] M. Şimşek and M. Al-shujairi. Static, free and forced vibration of functionally graded (FG) sandwich beams excited by two successive moving harmonic loads. *Composites Part B: Engineering*, **108**, (2017), pp. 18–34. https://doi.org/10.1016/j.compositesb.2016.09.098.

[11] T. H. Le, B. S. Gan, T. H. Trinh, and D. K. Nguyen. Finite element analysis of multi-span functionally graded beams under a moving harmonic load. *Mechanical Engineering Journal*, **1**, (3), (2014), pp. CM0013–CM0013. https://doi.org/10.1299/mej.2014cm0013.

[12] I. Esen. Dynamic response of a functionally graded Timoshenko beam on two-parameter elastic foundations due to a variable velocity moving mass. *International Journal of Mechanical Sciences*, **153**, (2019), pp. 21–35. https://doi.org/10.1016/j.ijmecsci.2019.01.033.

[13] I. Esen. Dynamic response of functional graded Timoshenko beams in a thermal environment subjected to an accelerating load. *European Journal of Mechanics - A/Solids*, **78**, (2019). https://doi.org/10.1016/j.euromechsol.2019.103841.

[14] I. Esen, M. A. Eltaher, and A. A. Abdelrahman. Vibration response of symmetric and sigmoid functionally graded beam rested on elastic foundation under moving point mass. *Mechanics Based Design of Structures and Machines*, **51**, (2023), pp. 2607–2631. https://doi.org/10.1080/15397734.2021.1904255.

[15] B. S. Gan, T.-H. Trinh, T.-H. Le, and D.-K. Nguyen. Dynamic response of non-uniform timoshenko beams made of axially fgm subjected to multiple moving point loads. *Structural Engineering and Mechanics, An International Journal*, **53**, (5), (2015), pp. 981–995. https://doi.org/10.12989/sem.2015.53.5.981.

[16] D. K. Nguyen, A. N. T. Vu, N. A. T. Le, and V. N. Pham. Dynamic behavior of a bidirectional functionally graded sandwich beam under nonuniform motion of a moving load. *Shock and Vibration*, **2020**, (2020). https://doi.org/10.1155/2020/8854076.

[17] D. K. Nguyen, T. T. Tran, V. N. Pham, and N. A. T. Le. Dynamic analysis of an inclined sandwich beam with bidirectional functionally graded face sheets under a moving mass. *European Journal of Mechanics - A/Solids*, **88**, (2021). https://doi.org/10.1016/j.euromechsol.2021.104276.

[18] Ş. D. Akbaş, Y. A. Fageehi, A. E. Assie, and M. A. Eltaher. Dynamic analysis of viscoelastic functionally graded porous thick beams under pulse load. *Engineering with Computers*, (2022), pp. 1–13. https://doi.org/10.1007/s00366-020-01070-3.

[19] K. Yee, U. M. Kankanamalage, M. H. Ghayesh, Y. Jiao, S. Hussain, and M. Amabili. Coupled dynamics of axially functionally graded graphene nanoplatelets-reinforced viscoelastic shear deformable beams with material and geometric imperfections. *Engineering Analysis with Boundary Elements*, **136**, (2022), pp. 4–36. https://doi.org/10.1016/j.enganabound.2021.12.017.

[20] Y. Cui, T. Zeng, M. Fan, R. Wu, G. Xu, X. Wang, and J. Zhao. Dynamic analysis of viscoelastic functionally graded porous beams using an improved Bernstein polynomials algorithm. *Chaos, Solitons & Fractals*, **189**, (2024). https://doi.org/10.1016/j.chaos.2024.115698.

[21] J. B. Kosmatka. An improved two-node finite element for stability and natural frequencies of axial-loaded Timoshenko beams. *Computers and Structures*, **57**, (1995), pp. 141–149. https://doi.org/10.1016/0045-7949(94)00595-t.

[22] M. Geradin and D. J. Rixen. *Mechanical vibrations: Theory and application to structural dynamics*. Wiley, 3rd edition, (2015).

[23] K. Henchi, M. Fafard, G. Dhatt, and M. Talbot. Dynamic behaviour of multi-span beams under moving loads. *Journal of Sound and Vibration*, **199**, (1997), pp. 33–50. https://doi.org/10.1006/jsvi.1996.0628.